Dalton Transactions

PAPER

View Article Online
View Journal | View Issue

Cite this: *Dalton Trans.*, 2018, **47**, 16211

Received 11th September 2018,
Accepted 22nd October 2018

DOI: 10.1039/c8dt03672a

rsc.li/dalton

A magnetic study of a layered lanthanide hydroxide family: $Ln_8(OH)_{20}Cl_4 \cdot nH_2O$ (Ln = Tb, Ho, Er)†

Joana T. Coutinho,[a,b] Claudia C. L. Pereira,[c] Joaquim Marçalo,[a,d] José J. Baldoví,*[e] Manuel Almeida,[a] Bernardo Monteiro*[a,d] and Laura C. J. Pereira*[a]

Three layered lanthanide hydroxides (LLHs), with the general formula $Ln_8(OH)_{20}Cl_4 \cdot nH_2O$ (Ln = Tb (**1**), Ho (**2**), Er (**3**)), were prepared and magnetically characterized both as pure compounds and diluted within a yttrium diamagnetic matrix, LYH : *x*Ln, LYH : 0.044Tb (**1′**), LYH : 0.045Ho (**2′**), and LYH : 0.065Er (**3′**). This study was complemented with theoretical calculations in order to understand the electronic configuration and the contributions to the slow relaxation behavior. In the pure compounds dominant 3D ferromagnetic interactions are observed, with a small magnetization hysteresis at 1.8 K for **1**, while the magnetically diluted solid solutions display slow relaxation of magnetization at low temperatures.

Introduction

The chemical design of multifunctional layered compounds, such as layered double hydroxides (LDHs), is nowadays one of the most attractive topics in materials science. These types of materials cover a broad range of possibilities,[1,2] from environmental and biomedical[3,4] to technological applications,[5] due to their compositional flexibility, since the identity of both cations and anions can be controlled to target a specific functionality.[3,6]

A particular class of these lamellar compounds are the so-called layered lanthanide hydroxides (LLHs) with the general formula $Ln_2(OH)_{6-m}(A^{x-})_{m/x} \cdot nH_2O$ (A refers to the intercalated anion and $1.0 \leq m \leq 2.0$), only containing lanthanide cations (Ln^{3+}) in the host layers. The first family of LLHs was reported by Gándara *et al.* in 2006, comprising rigid organic anions intercalated between inorganic layers[7] and since then dozens of LLH compounds have been reported.[8] These materials combine the layered structure with the high potential of lanthanide ions for different technological applications such as luminescent devices, catalysts, high-performance magnets and other functionalities.[8–10]

Although research on LLHs has been mainly focused on optical properties,[11–13] the magnetic properties of these lanthanide materials are also potentially interesting. Indeed the field of lanthanide-based mononuclear single-molecule magnets (SMMs), also known as single-ion magnets (SIMs), is nowadays one of the hottest research areas in molecular nanomagnetism.[14,15] Lanthanide based SMMs, which exhibit slow relaxation of magnetization and magnetic hysteresis below a certain blocking temperature (T_B), have recently achieved record values of T_B = 60 K, with an effective barrier (U_{eff}) above 1800 K, in a dysprosocenium complex.[16,17] Nevertheless, the magnetic properties of LLHs still remain largely unexplored, with the exceptions of our recent investigations on the SMM behavior in Dy layered compounds[18,19] belonging to the $Ln_8(OH)_{20}Cl_4 \cdot nH_2O$ series whose synthesis was previously reported by Geng *et al.* in 2008 [20,21] and the study of magnetocaloric properties of Gd-LLH.[22] In the former case, the evolution of magnetic interactions with growing dimensionality was investigated by comparison with the corresponding intercalated layered material and the yttrium diluted analogue. This permitted one to distinguish between the single-ion effects and those that result from 3D, 2D and Dy–Dy interactions.[18,19] Consequently, two distinct slow relaxation processes of magnetization below T_B present in this compound

---

[a] Centro de Ciências e Tecnologias Nucleares (C2TN), Instituto Superior Técnico, Universidade de Lisboa, Campus Tecnológico e Nuclear, Estrada Nacional 10, 2695-066 Bobadela, Portugal. E-mail: bernardo.monteiro@ctn.tecnico.ulisboa.pt
[b] Instituto de Ciencia Molecular (ICMol), Universidad de Valencia, Catedrático José Beltrán 2, 46980 Paterna, Valencia, Spain
[c] LAQV-REQUIMTE, Dep. de Química, Universidade Nova de Lisboa, 2829-516 Monte de Caparica, Portugal
[d] Centro de Química Estrutural (CQE), Instituto Superior Técnico, Universidade de Lisboa, Campus Tecnológico e Nuclear, Estrada Nacional 10, 2695-066 Bobadela, Portugal
[e] Max Planck Institute for the Structure and Dynamics of Matter, Luruper Chaussee 149, D-22761 Hamburg, Germany

† Electronic supplementary information (ESI) available. See DOI: 10.1039/c8dt03672a

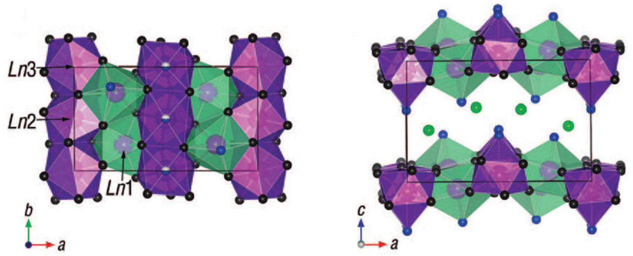

Fig. 1 $Ln_8(OH)_{20}Cl_4 \cdot nH_2O$ unit cell viewed along the *c* axis (left) and the *b* axis (right). Ln atoms are depicted as purple balls, hydroxyls as grey balls, water molecules as blue balls, and chloride ions as green balls. The 8-fold dodecahedron and 9-fold monocapped square antiprism are in light green and purple, respectively (adapted from ref. 20).

could be ascribed to the two main types of Dy sites observed in the crystal structure (Fig. 1).

Aiming at understanding the underlying parameters that rule this behavior, the study was extended to other lanthanide ions with potential magnetic properties within the $Ln_8(OH)_{20}Cl_4 \cdot nH_2O$ family (Ln = Tb (**1**), Ho (**2**), Er (**3**)) and their corresponding magnetically diluted solid solutions (LYH : *x*Ln; **1′**–**3′**). Thus, herein we report a detailed magneto-structural characterization of these compounds, exploring the effects of different magnetic moments.

Experimental

General information

The starting materials $LnCl_3 \cdot 6H_2O$ (Aldrich) (Ln = Y, Tb, Ho, Er), NaCl (Panreac), hexamethylenetetramine (HMT) (Aldrich) and 2,6-naphthalenedicarboxylic acid (Aldrich) were obtained from commercial sources and used as received.

Synthesis

The preparation of the undiluted LLH compounds (**1**–**3**) followed the original procedure described by Geng *et al.*,[20] which consists of the homogeneous precipitation of the desired $LnCl_3 \cdot xH_2O$ with hexamethylenetetramine.

***LTbH* (*1*)** *$Tb_8(OH)_{20}Cl_4 \cdot 5H_2O$*. A mixture of $TbCl_3 \cdot 6H_2O$ (1.859 g; 5 mmol), NaCl (3.799 g; 65 mmol), and HMT (0.701 g; 5 mmol) was dissolved in 1000 cm^3 of decarbonated Milli-Q water, and the solution was heated at refluxing temperature overnight under continuous magnetic stirring and nitrogen gas protection. The obtained final product was recovered by filtration, washed with deionized and decarbonated water and dried at 80 °C. Anal. calcd for $Tb_8(OH)_{20}Cl_4 \cdot 6H_2O$ (%): H, 1.73; Tb, 68.37. Found (%): H, 1.84; Tb, 68.43.

LHoH (2) $Ho_8(OH)_{20}Cl_4 \cdot 5H_2O$ was prepared as above but using $HoCl_3 \cdot 6H_2O$ (1.889 g; 5 mmol) for the reaction mixture. Anal. calcd for $Ho_8(OH)_{20}Cl_4 \cdot 6H_2O$ (%): H, 1.69; Ho, 69.17. Found (%): H, 1.78; Ho, 69.09.

LErH (3) $Er_8(OH)_{20}Cl_4 \cdot 5H_2O$ was prepared as above but using $ErCl_3 \cdot 6H_2O$ (1.894 g; 5 mmol) for the reaction mixture. Anal. calcd for $Er_8(OH)_{20}Cl_4 \cdot 6H_2O$ (%): H, 1.68; Er, 69.30. Found (%): H, 1.93; Er, 69.25.

The solid solutions LYH : *x*Ln (**1′**–**3′**) were prepared under identical conditions but with $YCl_3 \cdot xH_2O$ and $LnCl_3 \cdot xH_2O$ in the desired proportions for the reaction mixture, and the final product was dried under reduced pressure at room temperature.[19] All these compounds were obtained in good yields.

LYH : 0.044Tb (1′): anal. calcd for $Y_{7.65}Tb_{0.35}(OH)_{20}Cl_4 \cdot 6H_2O$ (%): H, 2.44; Tb, 4.20; Y, 51.38. Found (%): H, 2.65; Tb, 4.18; Y, 51.43.

LYH : 0.045Ho (2′): anal. calcd for $Y_{7.64}Ho_{0.36}(OH)_{20}Cl_4 \cdot 6H_2O$ (%): H, 2.48; Ho, 4.45; Y, 50.92. Found (%): H, 2.57; Ho, 4.51; Y, 51.05.

LYH : 0.065Er (3′): anal. calcd for $Y_{7.48}Er_{0.52}(OH)_{20}Cl_4 \cdot 6H_2O$ (%): H, 2.41; Er, 6.44; Y, 49.65. Found (%): H, 2.60; Er, 6.52; Y, 49.60.

Characterization procedures

Microanalyses of C and H were performed on a CE Instruments EA1110 automatic analyzer. To guarantee the complete combustion of the samples, V_2O_5 was added during the analysis. The metal content was determined by ICP-AES at Laboratório de Análises, Faculdade de Ciências e Tecnologia, Universidade Nova de Lisboa. TGA curves were obtained using a thermal analyser TA Q500-2207, with a scanning rate of 5 K min^{-1}, with samples weighing around 8 mg in aluminum crucibles. Conventional XRPD data were collected at room temperature on a Panalytical X'Pert Pro diffractometer, with a curved graphite monochromator (Cu K_α radiation, λ = 1.54060 Å), and a flat-plate sample holder, in a Bragg–Brentano para-focusing optics configuration (45 kV, 40 mA). Samples were step-scanned in 0.01° 2θ steps with a counting time of 2 s per step.

SIMPRE software

For the rationalization of the magnetic properties the SIMPRE computational package,[23] introducing the atomic coordinates and the experimental magnetic susceptibility data of the compounds as an input was used. The two fitting parameters (D_r and Z_i) of the Radial Effective Charge (REC) model have been varied. A detailed explanation is provided in the ESI.†

Magnetic measurements

Magnetic susceptibility measurements were performed on fixed powder polycrystalline samples of about 35 mg, using a 7 Tesla S700X SQUID magnetometer (Cryogenic Ltd). DC susceptibility data measurements were performed at temperatures ranging from 1.7 to 300 K, and under an applied magnetic field of 100 G (except for compound **3′**, where a DC field of 500 G was applied). The paramagnetic susceptibilities were obtained after correction for the core diamagnetism estimated using the Pascal constants: $\chi_D = -444.8 \times 10^{-6}$ emu mol^{-1} (**1**, **2**), -436.8×10^{-6} emu mol^{-1} (**3**), -316.2×10^{-6} emu mol^{-1} (**1′**, **2′**), and -391.9×10^{-6} emu mol^{-1} (**3′**). Dynamic AC measurements for all the six compounds were taken using a MagLab 2000 system (Oxford Instruments) with an AC field of

5 Oe. The temperature dependence of the AC magnetic susceptibility was measured at different frequency values within the 10–10 000 Hz range under zero and at different applied DC static fields (500 Oe, 1, 2, and 3 kOe). Additional isothermal AC susceptibility measurements, $\chi_{AC} = f(\omega)$, were taken in the same frequency range, within 1.7 to 12 K.

Results and discussion

Structural description

The ICP-AE analysis confirmed that the solid material obtained has Y : Ln ratios close to the composition of the starting solutions. The powder X-ray diffraction patterns of LLHs (**1–3**) are consistent with the crystallographic data published for the same compounds,[24] the diluted compounds (**1′–3′**) being identical to the Y derivative (Fig. S1–S7 in the ESI†). The Le Bail structureless whole pattern fitting, using the Powder Cell program, confirmed that the compounds prepared correspond to the same solid phases already reported. A slightly higher degree of crystallinity is observed in the solid solutions (**1′–3′**), most probably as a result of the different drying procedure. The H content was verified by elemental analyses and confirmed by thermogravimetry (TGA) measurements performed for all six compounds. From the plots (Fig. S8 in the ESI†) the expected decomposition behavior was observed by the presence of two regions of mass loss, one until *ca.* 473 K attributed to the loss of coordinated water molecules (calcd 4.7–4.8% for **1–3**, found 5.0–5.3%; calcd 8.1–8.2 for **1′–3′**, found 7.8–8.9) and another between 488 and 623 K due to the dehydroxylation of the hydroxide host layer.[25,26]

LLHs present, across the Sm–Er and Y series, an isostructural orthorhombic layered structure featuring positively charged layers, $[Ln_8(OH)_{20}(H_2O)_n]^{4+}$, with interlayer charge-balancing anions (Cl^- ions in this work). The in-plane lattice parameters *a* and *b* decrease almost linearly with the decrease of the Ln^{3+} ionic radius. As shown in Fig. 1, the unit cell of these materials contains three crystallographic distinct lanthanide sites, with two different Ln coordination environments, labelled as Ln1, Ln2 and Ln3. The layers are composed of edge-shared $[Ln(OH)_7(H_2O)]$ and $[Ln(OH)_8(H_2O)]$ polyhedra with each hydroxyl acting as a μ_3-bridge connecting the lanthanide centers and the chloride anions intercalated between the layers for charge balance.

Magnetic measurements

Static magnetic susceptibility measurements for LYH : *x*Ln and LLH materials are reported in Fig. 2 and S9,† respectively. The zero-field-cooled (ZFC) and field-cooled (FC) curves show a perfect overlap, with no indication of any ordering down to 2 K, as previously described for pure LDyH.[18] The χT values of all derivatives (diluted and undiluted ones) are slightly below those expected for the ground multiplets of Tb^{3+} (11.82 emu K mol^{-1}), Dy^{3+} (14.17 emu K mol^{-1}), Ho^{3+} (14.07 emu K mol^{-1}) and Er^{3+} (11.48 emu K mol^{-1}).[27] The diluted compounds (Fig. 2) show upon cooling a continuous slow decrease of χT, due to the progressive thermal depopulation of the excited M_J energy levels of the ground multiplet, as commonly observed in lanthanide compounds.[28,29] The slower decrease observed in the pure compounds can be ascribed to the presence of non-negligible Ln–Ln ferromagnetic interactions, as already reported.[18] These short-range ferromagnetic interactions appear to be more significant in the case of the Tb compound.

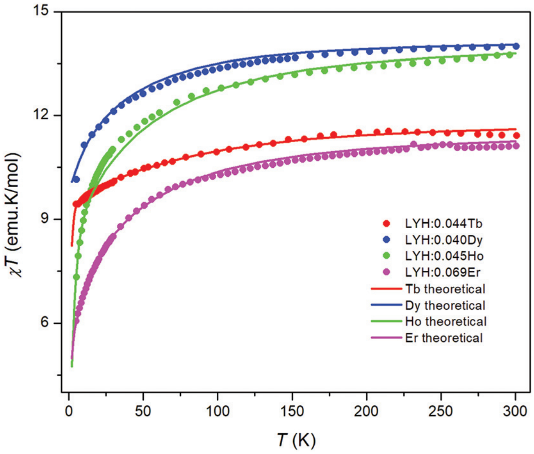

Fig. 2 Experimental data (symbols) and theoretical simulation (lines) of the temperature dependence of the magnetic susceptibility of LYH : *x*Ln (Ln = Tb (**1′**), Dy,[20,21] Ho (**2′**) and Er (**3′**)).

As can be observed in Fig. 2, the χT curves can be successfully reproduced by using the Radial Effective Charge (REC) model[30] in the SIMPRE[23,31] software package. The simultaneous fit of the four curves, using the different crystallographic coordination environments around each lanthanide ion leads to D_r = 1.17 Å and Z_i = 0.04. Both parameters were subsequently refined by slight variations (see Table S5†) in order to improve the phenomenological description. For the **Dy** and **Er** derivatives (Tables S7 and S10†), this approach gives a ground state wave function with a large contribution of a high M_J in **Dy2** (89% of $|\pm 15/2\rangle$) and **Dy3** (92% of $|\pm 15/2\rangle$), and **Er1** and **Er3** (99% and 100% of $|\pm 13/2\rangle$) in their respective easy axes. These contributions are in principle compatible with the SMM behavior observed in both compounds. Although families with Dy and Er analogues having simultaneously a ground state, as determined by a relatively large M_J value, have been previously reported,[32,33] it is important to remark the role of the actual charge distribution around the lanthanide in order to define the magnetic anisotropy of the system. These contributions are in principle compatible with the SMM behavior observed in both compounds. In the case of **Tb** and **Ho** (Tables S6 and S8†), the ground states are mainly diamagnetic, except for **Tb3** that stabilizes $M_J = \pm 6$, which can be responsible of the ferromagnetic interactions observed in **1**. The resulting energy levels and wave functions for each center are available in the ESI (Tables S6–S9†).

Isothermal magnetization measurements were performed at low temperatures using field sweeping rates of 20 and 90 Oe s^{-1}. The curve *M vs. H* for compound **1** is shown in

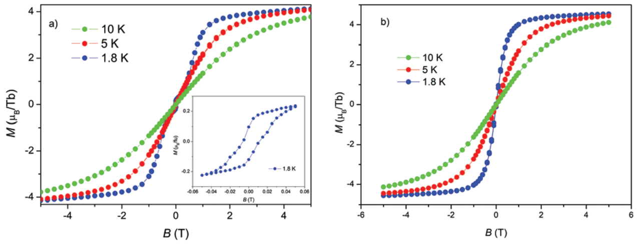

Fig. 3 Field dependence of the magnetization at several temperatures for (a) LTbH (**1**) with a field sweep of 20 Oe s^{-1} (inset corresponds to the enlarged curve at 1.8 K around zero field) and (b) LYH : 0.044Tb (**1′**) with a field sweep of 90 Oe s^{-1}.

Fig. 3a, where the existence of a magnetic hysteresis at low magnetic fields can be observed with a coercive field of about 200 Oe at 1.8 K. This curve shows a two-step shape, reaching first a magnetization of approximately $0.25\mu_B$ at 500 G, followed by a second step, where M rapidly increases to $3.8\mu_B$ at 20 kG and finally reaches $4.13\mu_B$ at 50 kG. This two-step behavior was also observed in the Dy analogue[18] and is most likely a reminiscence of metamagnetism associated with a spin-canting process, as often also found in layered materials.[34,35] The diluted compound **1′** (Fig. 3b), as well as both **Ho** (Fig. S10†) and **Er** compounds (Fig. S11†), did not show magnetic hysteresis nor any sign of a two-step process, indicating that these are originating from Tb–Tb interactions.[36] The presence of significant magnetic anisotropy and/or low-lying excited states[37] was confirmed by the non-superimposition of the M *vs.* B/T curves on a single master curve (Fig. S12†).

Dynamic magnetic measurements (AC) were taken at zero DC field and under static fields. At 1.7 K the optimal value for DC field, corresponding to the slowest relaxation time, was found to be 1000 Oe for all these compounds. Therefore both temperature and frequency dependence measurements were collected under zero and at H_{DC} = 1000 Oe.

For compound **1** the temperature dependence of both real and imaginary components of AC susceptibility, χ' and χ'' (Fig. S13†), taken under a zero static field showed a very sharp peak below 4 K. At different frequency values, these peaks slightly shift to higher temperatures and decrease their intensity, following a behavior characteristic of slow magnetic relaxation. However, when a DC field of 1000 Oe is applied the signal of both χ' and χ'' drastically changes with their maxima less pointed and smaller in magnitude (Fig. S14†). As previously indicated by the static magnetic measurements (Fig. 3) and the theoretical calculations this behavior also suggests the presence of some ferromagnetic characteristic due to the existing 3D Tb–Tb interactions. Measurements of the frequency dependence of the AC susceptibility were also performed for **1** but unfortunately the poor statistics of the measurements did not allow obtaining reasonable fits for the Cole–Cole plots. For compounds **2** and **3** at zero DC field no frequency dependence was observed and the data obtained under a static field of 1000 Oe was almost not frequency dependent (Fig. S15†). In contrast, the diluted compounds **1′**, **2′**, and **3′** present, although weak, a frequency-dependent response in zero DC field (Fig. S16–S18 in the ESI†). This behavior is clearly enhanced with the application of a static magnetic field (Fig. S19–S21†), although the appearance of resolved maxima is only observed for the compound with Er, **3′**.

In order to further characterize the magnetization relaxation rate, χ' and χ'' were isothermally measured while the frequency, ω, of the AC field was varied from 10 Hz to 10 kHz under a DC field of 1000 Oe. As seen in Fig. 4, these data

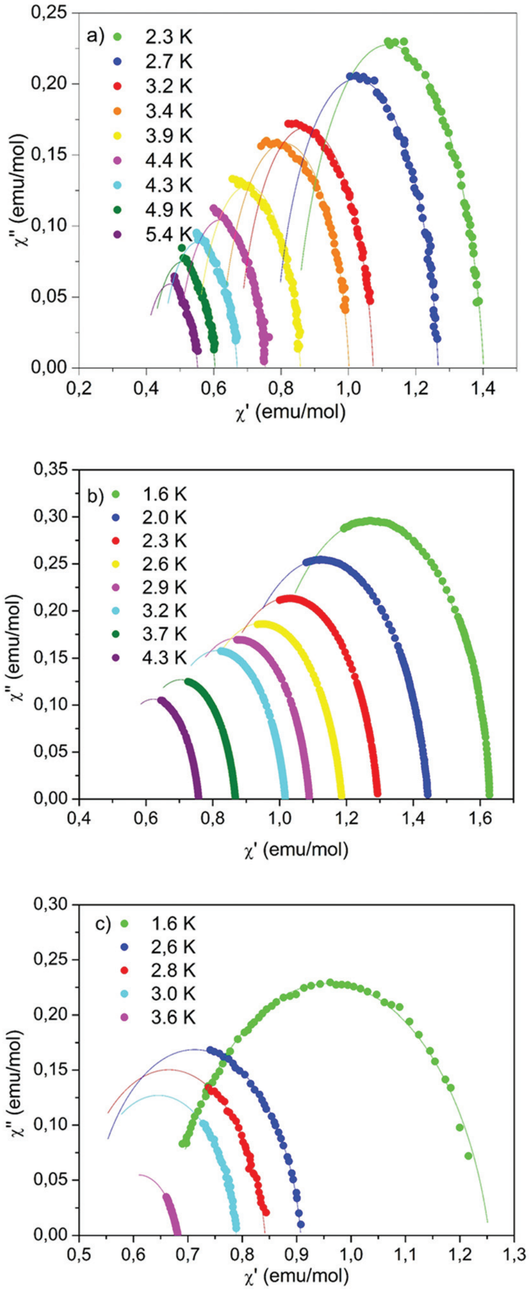

Fig. 4 Argand diagrams (dots) and Debye fittings (lines) of the AC susceptibility for compounds (a) **1′** (LYH : 0.044Tb), (b) **2′** (LYH : 0.045Ho), and (c) **3′** (LYH : 0.065Er) at different temperatures and under a static field of H_{DC} = 1000 Oe. H_{AC} = 5 Oe.

allowed the representation of Argand plots, χ'' *vs.* χ', at several fixed temperatures that show a good agreement when fitted to a modified Debye model (eqn (1) and Tables S1–S3†):

$$\chi_{\mathrm{ac}}(\omega) = \chi_{\mathrm{S}} + (\chi_{\mathrm{T}} - \chi_{\mathrm{S}})[1/1 + (i\omega\tau)^{1-\alpha}] \tag{1}$$

where χ_{S} and χ_{T} are the adiabatic and isothermal susceptibilities respectively, τ is the average magnetization relaxation time and α is a parameter ranging from 0 to 1 related to the width of the distribution ($\alpha = 0$ corresponds to the ideal Debye model, with a single relaxation time).

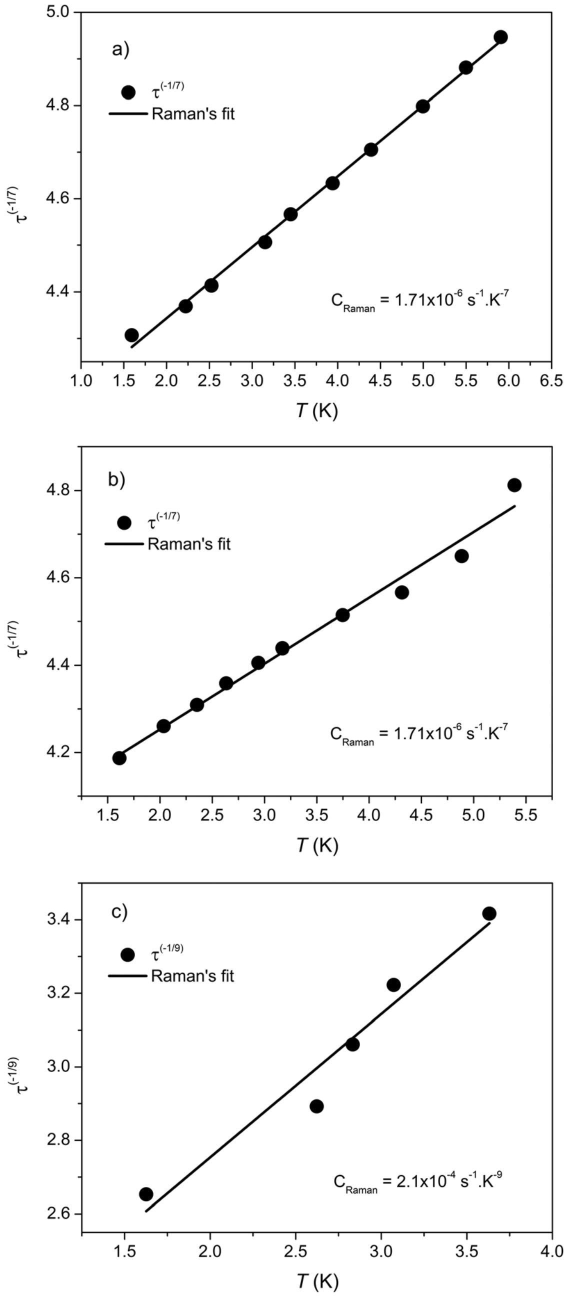

Fig. 5 Plot of the temperature dependence of the relaxation time, as $1/\sqrt[n_R]{\tau}$ *vs. T*, measured under H_{AC} = 5 Oe, H_{DC} = 1000 Oe for (a) **1**, (b) **2**, and (c) **3**. Lines correspond to the best fits for eqn (2) regarding the Raman process. In all cases, the fits have been plotted with a significant least squares result ($r^2 > 0.99$).

The small α values obtained ($\alpha \leq 0.2$) along with the semi-circular and symmetrical shape of the Argand diagrams are consistent with only one single magnetization process (Fig. 5 and Tables S1–S3†), with a narrow distribution of relaxation times. It is worth mentioning that the relaxation behavior of these compounds is significantly different from the one observed in the dysprosium analogue (LYH : 0.04Dy),[19] where a more complex regime with two relaxation processes was obtained under a static field of 1000 Oe.

A first attempt was made to fit these data to the Arrhenius law by assuming only the Orbach relaxation process (see the ESI†). The values found for the energy barriers were considerably smaller than the one obtained for the analogue diluted Dy compound (U_{eff} = 31 K).[19] Also, the fits for all three compounds only cover the higher temperature range showing deviations from linearity at lower temperatures (Fig. S22†).

Thus, and similarly to what has been observed in other lanthanide compounds[19,38] the relaxation mechanism can preferably occur *via* a virtual state such as the Raman process, which can be mathematically described by eqn (2):

$$\tau_{\mathrm{Raman}}{}^{-1} = C_{\mathrm{Raman}} \times T^{n_{\mathrm{Raman}}} \tag{2}$$

In Kramers ions an exponent of $n = 9$ is expected, although different values can also be found due to the limitation of the Debye model describing phonons in molecular solids.[39] The best fits were obtained assuming $n_{\mathrm{R}} = 7$ for the non-Kramers ions Tb^{3+} and Ho^{3+}, and $n_{\mathrm{R}} = 9$ for the non-integer spin system (Kramers ion) Er^{3+}. These results can be seen in Fig. 5, where a linear dependence of $1/\sqrt[n_R]{\tau}$ *vs. T* is observed for all data points. The values for the Raman parameter (C_{Raman}) are as expected for a second-order Raman process.

Comparing to the Orbach process, it is clear that the Raman process is more adequate to interpret the relaxation magnetic behavior of the three compounds and consequently a pure Raman process can be considered.

These values were corroborated by the theoretical calculations for the ground multiplet energy levels calculated by the REC model (Tables S5, S7 and S8†).

Conclusions

We have shown that the layered lanthanide hydroxides with the general formula $\mathrm{Ln_8(OH)_{20}Cl_4 \cdot }n\mathrm{H_2O}$ (Ln = Tb (**1**), Ho (**2**), Er (**3**)) present Ln–Ln interactions that can hide the presence of slow relaxation of magnetization. This is mainly observed for the terbium compound, where the presence of short-range ferromagnetic interactions is responsible for the appearance of a hysteresis in the *M vs. H* curves due to some spin-canting process and also the sharp maxima in the out-of-phase component of the AC susceptibility at zero DC field, which disappear when an external field is applied.

These results without excluding the occurrence of slow magnetic relaxation highlight the presence of significant interactions between the Ln centers, similarly to the previously reported $Dy_8(OH)_{20}Cl_4{\cdot}6H_2O$. A clear slow relaxation behavior is observed only in the magnetically diluted solid solutions LYH : xLn, LYH : 0.044Tb (**1′**), LYH : 0.045Ho (**2′**), and LYH : 0.065Er (**3′**). This behavior is more evident for the erbium derivative, but in contrast to $Dy_8(OH)_{20}Cl_4{\cdot}6H_2O$ and its respective diluted analogue, only one relaxation process is observed. This can be due either to different specific energy levels involved or to the second process being changed to lower temperatures.

Semi-empirical calculations performed by using the REC model successfully allowed the access of the Ln electronic configurations and the respective contributions to the slow relaxation behavior of these LLHs as previously reported for the diluted and the intercalated Dy compounds[19] showing a diversity of magnetic behaviors.

Conflicts of interest

There are no conflicts of interest to declare.

Acknowledgements

We thank the Fundação para a Ciência e a Tecnologia (FCT) for financial support through the UID/Multi/04349/2013 project (C2TN), UID/QUI/50006/2013 (LAQV-REQUIMTE), grants to J. T. C. (SFRH/BD/84628/2012) and C. C. L. P. (SFRH/BPD/108959/2015) and contract to BM (contract n° IST-ID/077/2018). We thank the EU for project "SunStorage- Harvesting and storage of solar energy" (POCI-01-0145-FEDER-016387), funded by European Regional Development Fund (ERDF) and co-financed by the ERDF under the PT2020 Partnership Agreement (POCI-01-0145-FEDER – 007265), through COMPETE 2020 – Operational Programme for Competitiveness and Internationalization (OPCI), (COST Action CA15128 MOLSPIN and ERC-2014-CoG-647301 DECRESIM) and the Spanish MINECO (Unit of excellence "Maria de Maeztu" MDM-2015-0538). J. J. B. thanks the EU for a Marie Curie Fellowship (H2020-MSCA-IF-2016-751047).

Notes and references

1 F. Leroux and C. Taviot-Guého, *J. Mater. Chem.*, 2005, **15**, 3628.
2 Q. Wang and D. O'Hare, *Chem. Rev.*, 2012, **112**, 4124.
3 L. Mohapatra and K. Parida, *J. Mater. Chem. A*, 2016, **4**, 10744.
4 C. Del Hoyo, *Appl. Clay Sci.*, 2007, **36**, 103.
5 V. Rives, *Layered Double Hydroxides: Present and Future*, Nova Science Publishers, Inc., New York, 2001.
6 G. Abellán, E. Coronado, C. Martí-Gastaldo, A. Ribera, J. L. Jordá and H. García, *Adv. Mater.*, 2014, **26**, 4156.
7 F. Gándara, J. Perles, N. Snejko, M. Iglesias, B. Gómez-Lor, E. Gutiérrez-Puebla and M. Á. Monge, *Angew. Chem., Int. Ed.*, 2006, **45**, 7998.
8 Qi Zhu, X. Wang and J.-G. Li, *J. Adv. Ceram.*, 2017, **6**, 177.
9 K. Binnemans, *Chem. Rev.*, 2009, **109**, 4283.
10 J.-C. G. Bünzli, *Acc. Chem. Res.*, 2006, **39**, 53.
11 Y.-S. Yoon, B.-I. Lee, K. S. Lee, G. H. Im, S.-H. Byeon, J. H. Lee and I. S. Lee, *Adv. Funct. Mater.*, 2009, **19**, 3375.
12 Y. Xiang, X.-F. Yu, D.-F. He, Z. Sun, Z. Cao and Q.-Q. Wang, *Adv. Funct. Mater.*, 2011, **21**, 4388.
13 C. C. L. Pereira, J. C. Lima, A. J. Moro and B. Monteiro, *Appl. Clay Sci.*, 2017, **146**, 216.
14 L. Escalera-Moreno, J. J. Baldovi, A. Gaita-Arino and E. Coronado, *Chem. Sci.*, 2018, **9**, 3265.
15 S. T. Liddle and J. van Slageren, *Chem. Soc. Rev.*, 2015, **44**, 6655.
16 C. A. P. Goodwin, F. Ortu, D. Reta, N. F. Chilton and D. P. Mills, *Nature*, 2017, **548**, 439.
17 F.-S. Guo, B. M. Day, Y.-C. Chen, M.-L. Tong, A. Mansikkamäki and R. A. Layfield, *Angew. Chem., Int. Ed.*, 2017, **56**, 11445.
18 B. Monteiro, C. C. L. Pereira, J. T. Coutinho, L. C. J. Pereira, J. Marçalo and M. Almeida, *Eur. J. Inorg. Chem.*, 2013, 5059.
19 B. Monteiro, J. T. Coutinho, C. C. L. Pereira, L. C. J. Pereira, J. Marçalo, M. Almeida, J. J. Baldoví, E. Coronado and A. Gaita-Ariño, *Inorg. Chem.*, 2015, **54**, 1949.
20 F. Geng, Y. Matsushita, R. Ma, H. Xin, M. Tanaka, F. Izumi, N. Iyi and T. Sasaki, *J. Am. Chem. Soc.*, 2008, **130**, 16344.
21 F. Geng, H. Xin, Y. Matsushita, R. Ma, M. Tanaka, F. Izumi, N. Iyi and T. Sasaki, *Chem. – Eur. J.*, 2008, **14**, 9255.
22 G. Abellán, G. M. Espallargas, G. Lorusso, M. Evangelisti and E. Coronado, *Chem. Commun.*, 2015, **51**, 14207.
23 J. J. Baldoví, J. M. Clemente-Juan, E. Coronado, A. Gaita-Ariño and A. Palii, *J. Comput. Chem.*, 2014, **35**, 1930.
24 F. Geng, Y. Matsushita, R. Ma, H. Xin, M. Tanaka, F. Izumi, N. Iyi and T. Sasaki, *J. Am. Chem. Soc.*, 2008, **130**, 16344.
25 X. Wu, J.-G. Li, J. Li, Q. Zhu, X. Li, X. Sun and Y. Sakka, *Sci. Technol. Adv. Mater.*, 2013, **14**, 015006.
26 F. Geng, Y. Matsushita, R. Ma, H. Xin, M. Tanaka, N. Iyi and T. Sasaki, *Inorg. Chem.*, 2009, **48**, 6724.
27 C. Benelli and D. Gatteschi, *Introduction to Molecular Magnetism: from transition metals to lanthanides*, Wiley-VCH, Weinheim, 2015.
28 (*a*) M. L. Kahn, J.-P. Sutter, S. Golhen, P. Guionneau, L. Ouahab, O. Kahn and D. J. Chasseau, *J. Am. Chem. Soc.*, 2000, **122**, 3413; (*b*) M. L. Kahn, R. Ballou, P. Porcher, O. Kahndagger and J.-P. Sutter, *Chem. – Eur. J.*, 2002, **8**, 525.
29 X.-L. Li, J. Wu, L. Zhao, W. Shi, P. Cheng and J. Tang, *Chem. Commun.*, 2017, **53**, 3026.
30 J. J. Baldoví, J. J. Borrás-Almenar, J. M. Clemente-Juan, E. Coronado and A. Gaita-Ariño, *Dalton Trans.*, 2012, **41**, 13705.
31 J. J. Baldoví, S. Cardona-Serra, J. M. Clemente-Juan, E. Coronado, A. Gaita-Ariño and A. Palii, *J. Comput. Chem.*, 2013, **34**, 1961.
32 M. A. AlDamen, S. Cardona-Serra, J. M. Clemente-Juan, E. Coronado, A. Gaita-Ariño, C. Martí-Gastaldo, F. Luis and O. Montero, *Inorg. Chem.*, 2009, **48**, 3467.

33 J. J. Baldoví, Y. Duan, R. Morales, A. Gaita-Arino, E. Ruiz and E. Coronado, *Chem. – Eur. J.*, 2016, **22**, 13532.

34 D. Shao, S.-L. Zhang, X.-H. Zhao and X.-Y. Wang, *Chem. Commun.*, 2015, **51**, 4360.

35 K. Bernot, J. Luzon, A. Caneschi, D. Gatteschi, R. Sessoli, L. Bogani, A. Vindigni, A. Rettori and M. G. Pini, *Phys. Rev. B: Condens. Matter*, 2009, **79**, 134419.

36 (*a*) N. Ishikawa, M. Sugita, T. Ishikawa, S.-y. Koshihara and Y. Kaizu, *J. Phys. Chem. B*, 2004, **108**, 11265; (*b*) M. R. Silva, P. Martín-Ramos, J. T. Coutinho, L. C. J. Pereira and J. Martín-Gil, *Dalton Trans.*, 2014, **43**, 6752.

37 (*a*) M. A. Aldamen, J. M. Clemente-Juan, E. Coronado, C. Martí-Gastaldo and A. Gaita-Ariño, *J. Am. Chem. Soc.*, 2008, **130**, 8874; (*b*) P.-P. Yang, X.-F. Gao, H.-B. Song, S. Zhang, X.-L. Mei, L.-C. Li and D.-Z. Liao, *Inorg. Chem.*, 2011, **50**, 720; (*c*) C.-S. Liu, M. Du, E. C. Sañudo, J. Echeverria, M. Hu, Q. Zhang, L.-M. Zhou and S.-M. Fang, *Dalton Trans.*, 2011, **40**, 9366.

38 (*a*) E. Lucaccini, L. Sorace, M. Perfetti, J.-P. Costes and R. Sessoli, *Chem. Commun.*, 2014, **50**, 1648; (*b*) Y. Rechkemmer, J. E. Fischer, R. Marx, M. A. Dörfel, P. Neugebauer, S. Horvath, M. Gysler, T. Brock-Nannestad, W. Frey and M. F. Reid, *J. Am. Chem. Soc.*, 2015, **137**, 13114; (*c*) S. Gómez-Coca, A. Urtizberea, E. Cremades, P. J. Alonso, A. Camón, E. Ruiz and F. Luis, *Nat. Commun.*, 2014, **5**, 4300; (*d*) J. T. Coutinho, B. Monteiro and L. C. J. Pereira, Ln(III) based SIMs, in *Lanthanide-based multifunctional materials*, ed. P. Martín-Ramos and M. R. Silva, Elsevier, Amsterdam, 2018, ch. 6, pp. 195–231, Paperback ISBN: 9780128138403.

39 C. A. Goodwin, F. Ortu, D. Reta, N. F. Chilton and D. P. Mills, *Nature*, 2017, **548**, 439.